

Wrinkling of freely floating smectic films

Kirsten Harth^{1,2}, Torsten Trittel¹, Kathrin May¹, and Ralf Stannarius¹

¹ Institute of Physics, Otto von Guericke University, 39106 Magdeburg, Germany,

² Universiteit Twente, Physics of Fluids and Max Planck Center for Complex Fluid Dynamics, P.O. Box 217, 7500 AE Enschede, The Netherlands

(Dated: July 6, 2022)

Wrinkling is a well known response of soft surfaces or thin sheets to lateral stresses or stress mismatches. Commonly, it represents a stable or metastable energy minimum of an elastically deformed structure. We demonstrate wrinkling as a transient dynamical pattern in thin freely floating liquid-crystalline films. Such films can develop a transient undulation instability or develop bulges in response to air-driven lateral compression of the membrane. Optical experiments with freely floating bubbles on parabolic flights and ground lab experiments are reported. The characteristic wavelengths of the wrinkles are in the submillimeter range. We demonstrate the dynamic origin of the pattern formation mechanism and develop a basic model for the wavelength selection and wrinkle orientation.

I. INTRODUCTION

Owing to their internal molecular layer structure, some smectic phases can form stable freely suspended films with submicrometer thickness and up to several centimeters in lateral extension. Smectic A and C phases exhibit fluid-like characteristics with regard to flow in the film plane. Such films have many features in common with soap films, and they can be prepared, similar to the latter, as closed bubbles [1–3]. At first glance, freely floating smectic bubbles appear very similar to soap bubbles, but they differ from them in some dynamic properties [4, 5], as a consequence of the layered molecular arrangement.

Any reduction of the local film surface requires the growth of the film thickness for volume conservation of the smectic material. The related reorganization of smectic layers is achieved in the thin films by the formation of so-called islands, viz. spots with additional layers on the film that are enclosed by dislocation arrays [1, 4–6]. Such a rearrangement represents a comparably slow process, it requires up to several hundred milliseconds. Thus, on short time scales these free-standing films are not able to respond to external forcing by thickness adaption. They retain a roughly constant surface area. When exposed to fast geometrical shape transformations, they are more similar to thin elastic sheets than to fluid films.

As we will show here, a very fast and efficient response to rapid shape changes of freely floating smectic films and bubbles is the formation of bulges and tubuli [5] or wrinkles. Thereby, the film surface remains roughly constant, yet the local deformations result in a reduction of the effective lateral extension of the film (shortly referred to as ‘film area’ in the following). In the present paper, we characterize this unique dynamic wrinkling and we describe the spontaneous formation of bulges and tubuli (as shown in Figs. 1,2). A model is derived that gives a qualitative explanation of the main features of the instability.

We performed most of the experiments in microgravity during parabolic flights, a few studies were carried out in the ground lab at normal gravity.

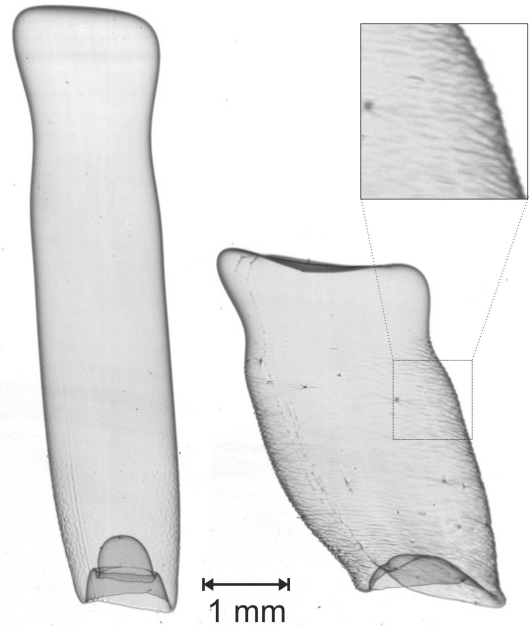


FIG. 1. Freely floating smectic bubble with homogeneous film thickness of 50 nm that is axially compressed by air flow. Thereby, it develops a wrinkled structure normal to the compression direction. The right hand image was recorded 50 ms after the left one. The bubble was produced under normal gravity, thus the pinch-off is asymmetric and the bottom part develops a typical invagination.

II. WRINKLING MECHANISMS

Before describing the experiment and data analysis, we give a short introduction into wrinkling mechanisms of thin elastic or fluid membranes: Wrinkles in soft matter systems can be of very different types, static and dynamic. Examples of static structures are skin wrinkles [7], drying fruit and vegetable peels, or stiff surface layers on shrinking elastic supports. They are quasi-static responses to stress balances. The latter also applies to

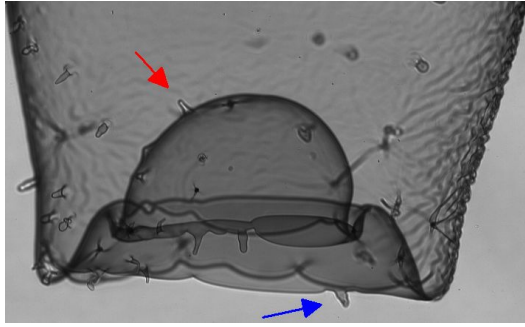


FIG. 2. Detail of a freely floating smectic bubble near the invagination at one end, with wrinkles and tubular extrusions that form during shape relaxation. Extrusions of the bubble can point inwards or outwards (see arrows). Wrinkles appear, for example, when the bubble is rapidly compressed in one or two directions. The image width is approximately 1 mm.

curtains or drapes, where the spontaneous crinkles reflect a compromise between gravitation energy and bending stiffness. Those structures represent stable or metastable energy minima.

Mechanically induced static layer undulations have also been discovered in smectic liquid crystals confined to thin sandwich cells with fixed boundary conditions. One example is the classical Helfrich-Hurault instability [8, 9]. It can occur in thin cells under dilation strain when the cell thickness is increased by external forcing. Layer undulations relieve smectic layer dilation, the elastic energy necessary for layer thickness changes competes with the elastic energy of director distortions induced by layer curvature. Wavelengths of those patterns are typically in the nanometer range. A similar instability can be produced in a fixed cell by means of electric or magnetic fields. These are conservative equilibrium patterns as well, representing free energy minima.

On the other hand, dynamic wrinkles can form, e. g. during a collapse of fluid bubbles in a gaseous environment. When a hemispherical bubble of highly viscous material sessile above a bulk bath ruptures, it can develop well-ordered wrinkles. The driving forces are gravitation and lateral confinement by the bubble geometry [10–12]. The formation of wrinkles of fluid interfaces have also been described during the impact of droplets onto a viscous liquid [13] and for droplets rising in a liquid [14]. A related phenomenon is the buckling of viscous fluid filaments [15, 16].

The structures described here are also of dynamical origin. They belong to the class of transient pattern forming instabilities. The smectic films undergo a rapid change from an initially flat geometry to an undulated shape. Thereby, a broad band of modes with different wavelengths becomes unstable, and the mode with the fastest growth rate dominates the periodicity of the pattern. We note that the area of the film-air interface does not change noticeably during this wrinkling process, we can disregard any surface-tension related forces.

The thickness of the films is typically in the range of a few dozen nanometers, much smaller than the observed wavelengths. Therefore we can treat the film as a quasi-twodimensional fluid sheet, surrounded by air on both sides. Because of the absence of sublayers with differing stiffnesses, and the absence of rigid boundaries at the film surfaces, the wrinkles described in our experiment are homogeneous across the films.

III. EXPERIMENTAL SETUP AND MATERIALS

Films were prepared from a room temperature smectic C mixture with 50 vol% of 2-(4-n-Hexyloxyphenyl)-5-n-octylpyrimidine and 50 vol% of 5-n-Decyl-2-(4-n-octyloxyphenyl) pyrimidine. The smectic C range is between 20 and 53 °C. We created the bubbles by a technique described earlier [4]: The two coaxial circular rings are wetted with the smectic substance, then brought in contact. After their slow separation with a stepper motor, a catenoid shaped smectic film is formed. Since the catenoid shape exists as an equilibrium film shape only up to a maximum ring separation of $D_{\text{crit}} \approx 1.3254 R$ (with the inner ring radius R), the catenoid collapses at this critical separation and leaves a freely floating, elongated bubble. This is sketched in Fig. 3. With rings between 20 mm and 25 mm radius, the bubbles have radii of a few millimeters. The catenoid collapse usually also leaves two circular films in the support rings which perform damped oscillations to equilibrium.

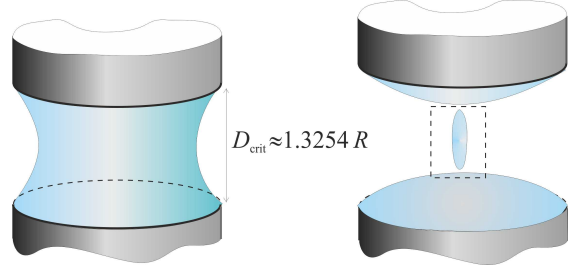


FIG. 3. Experimental geometry: two support rings and the catenoid before pinch-off (left) and the satellite bubble plus remnant films after pinch-off (right). The dashed rectangle sketches the maximum field of view of the side view camera. Most of the images shown in this paper are smaller clips of this field of view, focusing on details.

Experiments were performed in microgravity during parabolic flights at NOVESPACE (Bordeaux) with an Airbus 310, as well as in the ground lab under normal gravity. In both situations, bubbles form, but their properties differ in detail. Microgravity leads to a symmetric pinch-off of the upper and lower film parts, producing symmetric bubbles and a pair of films at the catenoid holders oscillating in antiphase. Those films periodically create air flow along the central axis that affects the bubble, squeezing and stretching it.

In normal gravity, the pinch-off is asymmetric, the bubbles usually pinch off at their upper end first. The initial bubble shapes, the relative phase of the film oscillations as well as the symmetry are affected. One problem with experiments under normal gravity is that the bubbles tend to leave the observation window rather fast.

The bubbles were observed with two high-speed cameras, providing a side view and a bottom view. Within this study, exclusively the side views recorded with a Phantom v710 camera (operated at 5,000 to 10,000 fps) were evaluated. We illuminated the bubbles with parallel light, using a blue high-power LED with wavelength 460 nm.

Wavelengths of the wrinkles were determined from 2D Fourier Transforms, where we restricted the evaluation to small areas normal to the viewing direction.

The thickness of the smectic film was measured with an adapted standard procedure that was developed for spherical smectic bubbles [17]. All films studied had submicrometer thicknesses, bubble diameters were in the millimeter to centimeter range.

IV. RESULTS AND DISCUSSION

A. Shape dynamics

As seen in Fig. 1 and sketched in Fig. 3, the bubbles have an elongated shape after pinch-off. They gradually transform into spheres with minimal surface during a period of several hundred milliseconds. This scenario has been analyzed in detail before [4]. On short time scales, however, the smectic films behave like membranes with zero surface tension and fixed surface area. During the shape transformations, the films permanently experience local compressions and dilations. Air flow around the bubbles advects the smectic film material and permanently forces the films to reorganize locally. The main reason for this air flow is the oscillation of the two remnant films at the support tubes (Fig. 3). It depends in a complex fashion on the amplitude and phase of the two oscillating films.

The flow induced in the smectic film by these friction forces can be locally divergent. Positive divergence either leads to local film thinning (rupture of some layers), or even to the rupture of the whole film [5]. In smectic C films, it may induce a reduction of the soft tilt angle [18]. Negative divergence compresses the film region. When the surface area of the film cannot be reduced quickly enough by island formation [5, 6], the films need to buckle out of the plane.

In addition, bubbles that are far from the equilibrium sphere shape can undergo complex shape transformations that involve local contraction of the bubble circumference.). They can also develop invaginations at their ends, whereby a part of the bubble membrane is pushed inwards (cf. Figs. 1,2). In all these cases, the film may be subject to lateral compression. The response of the films

is diverse and it depends upon the speed of the compression and on details of the film structure. If the compression is sufficiently slow, then the film remains flat and forms islands [6]. Fast compression cannot be compensated by this mechanism. Then, if islands already exist, the film reacts by local out-of-plane bulging of the islands as described in the next section. At higher compression rates, this process can be accompanied by wrinkling of the background film. If the film is uniformly thick, or if only very few islands exist, wrinkling is the dominant response.

B. Bulges and tubuli

Details of a bubble that is randomly speckled with islands of a few dozen micrometers diameter are shown in Fig. 4. There, the film reacts to the lateral compression with an extrusion of bulges at the centers of some islands. Arrows point at two selected features (islands/bulges) to visualize the axial contraction of the bubble. The open arrows indicate the expected positions of the second feature if the film had not contracted.

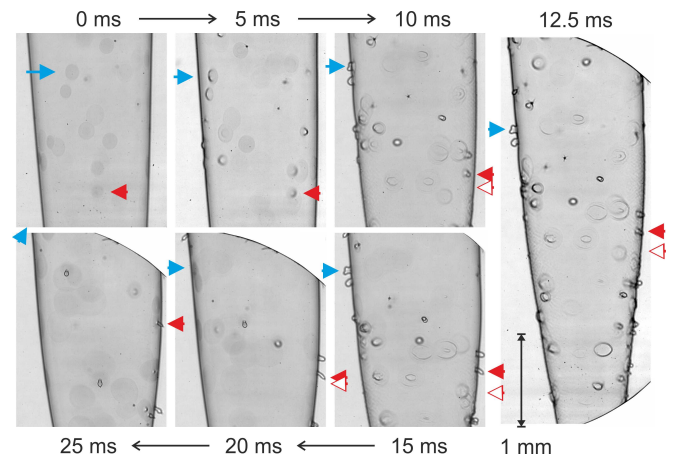


FIG. 4. Formation of bulges during the lateral compression of inhomogeneously thick films. The film has a background thickness of about 23 nm, islands of larger film thicknesses are seen as dark spots on the bubble. Times are given respective to the first image. The 12.5 ms image shows a larger part of the bubble. Whitened corners in some images mask the regions outside the observation window. We note that the whole bubble slightly spins counterclockwise (when seen from above), thus the features on the front continuously move to the right. Explanation of the arrows see text.

The islands represent 'germs', and bulges are formed in their centers (Figs. 4,5). Even though it seems natural that film thickness inhomogeneity breaks the translation symmetry and thus acts as local generators of deformations, it appears counterintuitive at first glance that the extrusions appear in the thicker parts of the film. Since the energy per area necessary to bend the smectic film is proportional to the film thickness (see next section),

islands are actually stiffer than the surrounding background film. Thus it should be easier to bend the thin background film rather than islands. A potential reason for the observed phenomenon is the line tension created by the dislocations surrounding an island, it generates an additional lateral compression force. This also explains why smaller islands are more probable to form bulges (cf. Fig. 5). The typical lateral extensions of the bulges are determined by the island sizes. The maximum diameters of bulges are of the order of the island diameters.

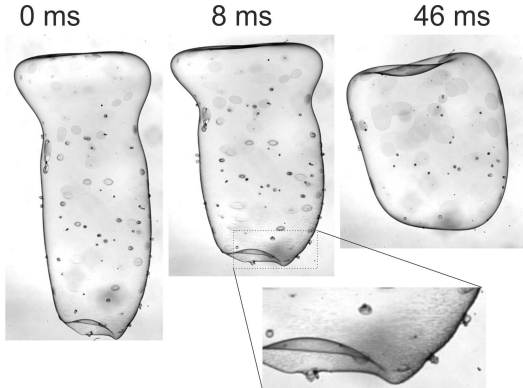


FIG. 5. Asymmetric bubble, background film thickness 16 nm: Bulges form only in the contracting regions. In the second image, taken 8 ms after the first one, shallow wrinkles form at the bottom end. The bottom image is a zoomed view of this region. After another 38 ms, the wrinkles dissolved and the bulges gradually disappear (right image).

The bulges form at a time scale of a few milliseconds. Figure 4 shows a typical image sequence of a contracting bubble section (in the first 15 ms). As long as the compression continues, the bulges grow and they can form tubuli which can even pinch off. When the exposed region stretches again, bulges disappear. This is seen in the second part of Fig. 4, for the following 10 milliseconds.

Figure 5 shows a bubble of exotic shape that contracts in the central and lower parts much more than in the upper part. Even though islands are uniformly distributed across the surface of this bubble, bulges are formed almost exclusively in the contracting central and lower regions. Islands in the top part, less exposed to contraction, remain flat. The third image shows the disappearance of the bulges during the expansion of the bubble diameter.

In flat films, the bulges can grow to both sides. In bubbles, the small excess pressure of a few Pascal inside the bubbles does not cause a preferential side of bulge formation, they can grow inward and outward. However, the local mean curvature of the film breaks the symmetry and provides a preference direction for bulging. Bulges and tubuli primarily grow outwards in regions where the local bubble surface is convex, this is common case, but they can also grow inwards where the local bubble surface is concave. This is exemplarily seen in Fig. 2.

C. Wrinkles

In bubbles of uniform film thickness, the film response is completely different, as shown in Fig. 6. The overall bubble geometry and shape dynamics are very similar to those in Fig. 4, except that there are practically no islands. This bubble section undergoes an axial contraction. The wrinkles form primarily perpendicular to the contraction direction. As in Fig. 4, arrows point at two selected features of the film to visualize the axial contraction of the bubble. The open arrows indicate the expected positions of the second feature if the film had not contracted.

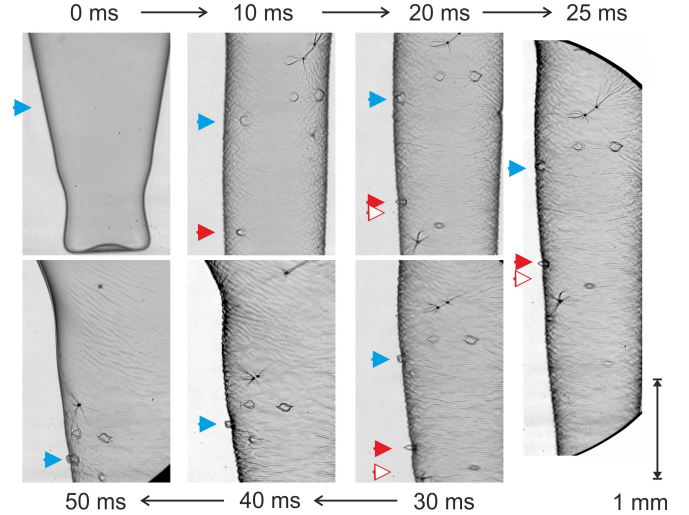


FIG. 6. Formation of wrinkles during the lateral compression of an almost homogeneously thick film. The film has a background thickness of about 32 nm. The images show a selected area of the bubble surface. Times are given respective to the first image. The 25 ms image shows a larger part of the bubble. Whitened corners mask the regions outside the observation window. Arrows mark selected features, in order to identify the corresponding film regions in subsequent images (see text and Fig. 4).

The film undulations can be directly seen in microscopic images at the sides of the bubble. Figure 7 shows a zoomed-in detail of the fully developed wrinkles. One recognizes that the amplitudes are of the same order of magnitude as the wavelengths.

When the contraction stress ceases, the wrinkles gradually disappear again (Fig. 6, bottom row). They can reappear at a subsequent new contraction. During wrinkling, the surface area stays practically constant, and the orientation of the wrinkles is directly coupled to the contracting direction.

Quantitatively, it is possible to measure the spectrum of the wrinkles by means of Fourier Transform (FT) of the optical images of certain bubble regions. In order to avoid distortions, it is recommendable to choose regions where the viewing direction is normal to the film. Figure 8 shows three snapshots of wrinkles and the cor-

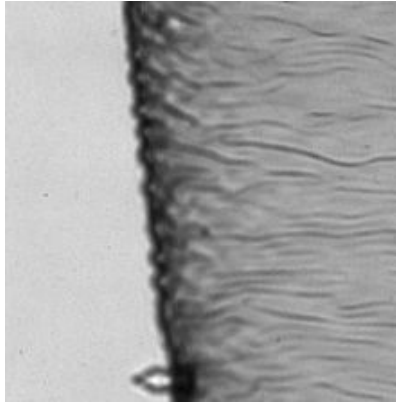


FIG. 7. Detail of the wrinkle structure in side view (zoom of the 25 ms image in Fig. 6).

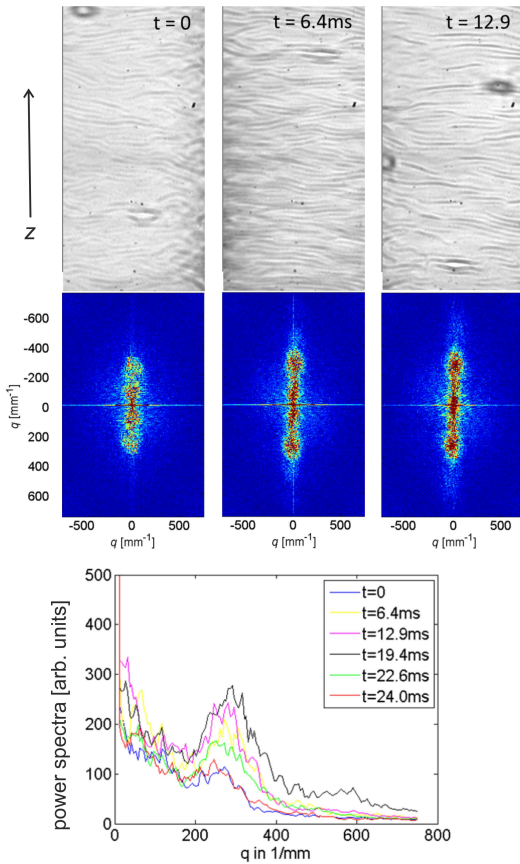


FIG. 8. Details of the wrinkles of an axially compressed bubble (top images) and vertical cross section profile of the Fourier Transforms. The contraction stops after 20 ms. Thereafter, the region expands again.

responding intensity of the 2D FT power spectrum. It is obvious from the spectra that the wrinkles show a high degree of orientational ordering. From the plot of the 2D cross sections of these spectra along the symmetry axis (vertical in the images) the graphs in the bottom image of Fig. 8 were obtained. It is evident that the spectrum

develops a characteristic peak around the wave number $q_{\max} \approx 300/\text{mm}$. This corresponds to wave lengths of about $20 \mu\text{m}$ of the wrinkles. Furthermore it is evident that the wave length decreases with time. This is the consequence of the material-fixed position of the wrinkles. The number of wrinkles in a certain film region remains approximately constant, and the maximum of the spectrum shifts to shorter wavelengths (larger q) as a consequence of the lateral compression of the structure.

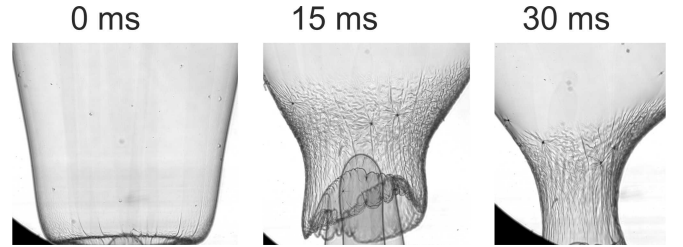


FIG. 9. Local contraction of the bubble diameter leads to axial wrinkles. The dark regions are outside the observation window. Image heights are 2 mm.

Another scenario where wrinkles can form is the contraction of a tubular bubble section, as seen in Fig. 9. Here, the wrinkles are generated with a preferential axial direction respective to the bubble. In that geometry, the divergence of air flow outside the bubble is practically irrelevant. The compression arises from the local shrinkage of the bubble circumference. Typical wavelengths appear to be slightly larger than in the former, tangential patterns. Often, the shape transformations of bubbles involve more complex scenarios, where both the axial contraction and the diameter shrinkage occur concurrently. In that case, less ordered patterns are observed. A typical example is that of Fig. 2 where wavelengths with different orientations are superimposed.

V. DYNAMIC WRINKLING MODEL

The model developed in this section is intended to describe the simple structures shown in Figs. 6, 7 and 8. Although the oscillation dynamics at least of simple soap bubbles seem to be fairly well understood [19], the complex air flow in the present system is largely unresolved. Even the very shape dynamics of the freely floating smectic bubbles have not been analyzed in detail, except for the quantitative analysis of shape deformations in special geometries [4–6]. In order to demonstrate the principal mechanism without providing a deeper quantitative analysis, we may therefore base our model on crude approximations.

The model assumes a rectangular film area of a given width B and length $L_0 = L(t = 0)$. This area is compressed by opposing forces \vec{F}_s along z and $-z$, resp. (Figure 10). The response of the film is the formation of N wrinkles with initial wavelength $\lambda_0 = L_0/N$ and

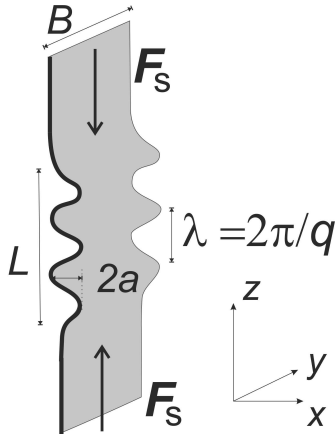


FIG. 10. Film geometry and definition of the coordinates.

amplitude a . Small deformations are approximated by $X(z) = a \sin qz$, with $q = 2\pi/\lambda$. The initial wavelength is $q_0 = 2\pi N/L_0$. During the compression, the number of wrinkles remains roughly conserved (wrinkles are material-fixed) and their wavelength decreases. Since we are interested in the initial wavelength selection process, we can safely set the wavelengths as constant, $q \approx q_0$.

We first consider the situation where the driving force F_s is caused by friction of the air flow, primarily outside the bubble. The force per width of the rippled film is $f_s = F_s/B$. This force performs a mechanical work W_s , which is on one hand stored in the deformation of the smectic film (W_b), on the other hand dissipated primarily by air flow related to the growth of the undulation amplitude (W_f). We thus set $W_f = W_s - W_b$. The mechanical work of the friction forces performed on the film is $W_s(t) = f_s B(L_0 - L(t))$. From the relation $L_0 = \int_0^L \sqrt{1 + (dX/dz)^2} dz$, one finds $L_0 \approx (1 + a^2 q^2/4)L$, thus

$$W_s = \frac{f_s B L}{4} a^2 q^2.$$

The reduction of the lateral film area (at given amplitudes a of the undulation) is more effective for shorter waves, this will provide damping of the long-wavelength tail of the unstable mode band.

Bending of smectic membranes is related to a free energy density contribution of the form

$$w_b = \frac{1}{2} K (X'')^2. \quad (1)$$

One of the main contributions to this term is the splay deformation of the director $\vec{n}(z)$,

$$w_{\text{elast}} = \frac{1}{2} K_{11} (\nabla \vec{n})^2 \quad (2)$$

which in the smectic A phase is linearly coupled to layer undulations

$$(\nabla \vec{n}) = \frac{dn_z}{dz} = -\frac{d^2 X}{dz^2}$$

in our geometry. In addition, we do not exclude other potential contributions to the smectic layer bending elasticity [20, 21]. For example, the layer compression modulus may have some influence, but since the deformation across the thin film is in good approximation uniform, we expect that these terms are irrelevant here. Probably, there are other contributions that are usually disregarded in literature, which may have the same functional form of Eq. (1), but the splay term seems to be the dominating one. Integrated over the wrinkled region, one obtains (with the averages $\sin^2 qz = \overline{\cos^2 qz} = 1/2$)

$$W_b = \frac{KLBh}{4} a^2 q^4, \quad (3)$$

where h is the film thickness. Of course, this model is strictly correct only for a smectic A film. It is only an approximation for the smectic C bubbles studied here. But since we are interested primarily in the qualitative elucidation of the instability mechanism, this detail may be of secondary importance. Earlier experiments [5] showed that it is much more difficult to obtain stable smectic A bubbles. They are much more vulnerable to bursting than the smectic C films investigated in our experiments.

Now, we need to relate the growth rate of the undulation to the flow of air from the crests to the valleys of the undulation wave, and consequently to the pressure profile $p(z)$ along the film. We can relate the pressure gradient profile with the air flow j_z along the film (z direction) by the equation

$$j_z = -Cp'(z), \quad (4)$$

where C is a geometrical constant that describes the complex flow processes redistributing the air along the bulging film. The quantitative determination of this constant is not straightforward, but we assume that it is roughly the same for all wavelengths. We consider a pressure modulation with the same periodicity as the film deflection, $p = p_0 \sin qz$. The local film deformation changes according to

$$\dot{X} = \frac{dj_z}{dz} = -Cp''(z). \quad (5)$$

This yields the relation between the growth of the deformation amplitude and the pressure amplitude

$$\dot{a} = Cq^2 p_0, \quad p = \dot{a}C^{-1}q^{-2} \sin qz \quad (6)$$

The energy dissipated in this process is

$$W_f = \int_0^L p dV = B \int_0^L p X dz. \quad (7)$$

Inserting Eq. (6) into the equation (7) for the dissipated energy W_f , we find

$$W_f = B \int_0^L C^{-1}q^{-2} \sin^2(qz) a \dot{a} dz, \quad (8)$$

and averaging $\overline{\sin^2 qz} = 1/2$ yields

$$W_f = \frac{BL}{2Cq^2} a\dot{a}. \quad (9)$$

We arrive at the dispersion relation

$$\dot{a} = (f_s q^2 - Kh q^4) \cdot \frac{C}{2} q^2 a = (f_s q^4 - Kh q^6) \frac{C}{2} a, \quad (10)$$

which describes exponential growth of an unstable mode band between $q = 0$ and $q_c = \sqrt{f_s/(Kh)}$. The fastest growing mode is

$$q_{\max} = \sqrt{\frac{2}{3} \frac{f_s}{Kh}}, \quad (11)$$

and the maximum growth rate is

$$s_{\max} = \frac{2C}{27} \frac{f_s^3}{K^2 h^2}. \quad (12)$$

Thinner films develop wrinkles faster than thicker ones. An estimate of f_s , with $K \approx 10$ pN, $h \approx 20$ nm, and $q_{\max} = 300$ mm $^{-1}$, is 3 nN/m. Such a force per film width may be provided, e. g., with a velocity gradient in air of 0.2 s $^{-1}$ and an area of attack of the friction forces of $B \times 1$ mm. For quantitative predictions on the growth rates, one would need a guess of the geometrical constant C . We can only make an estimate of $C \approx 10^{-3} \text{m}^5 \text{N}^{-1} \text{s}^{-1}$ from the experimental data and Eq. (12).

We summarize these results as follows: A lateral compression of the film that is faster than the time scale necessary to reorganize the film thickness leads to a growth of ripples within a certain mode band. The wrinkles are aligned with the wave vector along the compression forces. The fastest growing mode depends upon the bending rigidity of the film, the wave number becomes smaller with larger K . The wave number also decreases with film thickness, because the energy needed to buckle the film linearly increases with film thickness. Furthermore, the lateral force f_s is the essential ingredient for the development of the wrinkling instability. It needs to exceed a threshold set by Kh in order to achieve the formation of an unstable mode band with sufficiently quick growth rates. The larger f_s , the shorter are the wavelengths of the wrinkles. The forces F_s can arise from friction of a convergent air flow near the film surface. Their quantitative determination is complicated and was not attempted within this study. During the evolution of the instability, the dominant wave length shortens proportional to L/L_0 .

VI. CONCLUSIONS AND SUMMARY

We have demonstrated that smectic freely floating bubbles can exhibit a novel type of spontaneously formed dissipative pattern, the wrinkling of thin films. It occurs as a transient instability when such films are either exposed to convergent air flow or when a tube-like bubble section contracts. The patterns occur only when the films are exposed to strong compression stresses in the film plane. The film surface area remains approximately unchanged. When the compression stresses cease or transform into dilation stresses, the wrinkles disappear again. Typical timescales for growth and disappearance are few milliseconds. Typical wavelengths are in the range of a few dozen micrometers. It is obvious that this phenomenon cannot be observed in conventional soap films which can practically immediately react to lateral compression by thickness growth and area reduction. It is a peculiarity of the smectic structure.

The second phenomenon described here is the extrusion of bulges from the plane in films that contain islands. Here, a challenge will be the identification of the instability mechanism in detail, and a quantitative description of the relation between island sizes, line tensions, external compression forces and bulge sizes. A better spatial resolution in the experiment will be required for that.

A key ingredient of our experiment are the oscillating drum-like smectic membranes that remain at the catenoid holders and that produce strong air flows in axial direction, distorting the freely floating bubbles. More quantitative experiments may be possible if the bubbles are exposed to well-controlled acoustic excitation fields. This could be a challenging future task. The obvious reason that dynamic wrinkles have not been described before is that practically all earlier investigations of smectics, with few exceptions, have been performed either in sandwich cells with rigid interfaces or in thin free-standing films spanned across fixed supports.

Apart from the general relevance of this unique phenomenon, the patterns may provide quantitative access to material parameters of smectic LCs that are otherwise very difficult to measure. Future studies should be directed to the comparison of smectic C and smectic A phases.

ACKNOWLEDGMENTS

This study was performed with financial support from DLR within Project OASIS-Co (50WM1430) and from DFG (STA 425/40-1). Participation of Robert Göpfert and Vincent Nathow in the ground lab measurements is gratefully acknowledged.

[1] P.Oswald, "Dynamics of collapse of a smectic bubble," *J. Physique* **48**, 897–902 (1987).

[2] R. Stannarius and Ch. Cramer, "Surface tension measurements in freely suspended bubbles of thermotropic

smectic liquid crystals," *Liq. Cryst.* **23**, 371 (1997).

[3] R. Stannarius and Ch. Cramer, "Self-supporting bubbles of thermotropic smectic liquid crystals," *Europhys. Lett.* **42**, 43 (1998).

[4] K. May, K. Harth, T. Trittel, and R. Stannarius, "Dynamics of freely floating smectic bubbles," *Europhys. Lett.* **100**, 16003 (2012).

[5] K. May, K. Harth, T. Trittel, and R. Stannarius, "Freely floating smectic films," *ChemPhysChem* **15**, 1508 (2014).

[6] Patricia Dähmlow, Torsten Trittel, Kathrin May, Kirsten Harth, and Ralf Stannarius, "Surface reduction of freely-floating smectic bubbles," *Liquid Crystals* **45**, 993 (2018).

[7] E. Cerdá and L. Mahadevan, "Geometry and Physics of Wrinkling," *Phys. Rev. Lett.* **90**, 074302 (2003).

[8] H. Helfrich, "Deformation of cholesteric liquid crystals with low threshold voltage," *Appl. Phys. Lett.* **17**, 531 (1970).

[9] G. Bevilacqua and G. Napoli, "Reexamination of the helfrich-hurault effect in smectic-A liquid crystals," *Phys. Rev. E* **72**, 041708 (2005).

[10] G Debrégeas, P.G. de Gennes, and F Brochard-Wyart, "The life and death of "bare" viscous bubbles," *Science* **279**, 1704–1707 (1998).

[11] R da Silveira, S Chaïeb, and L Mahadevan, "Rippling instability of a collapsing bubble," *Science* **287**, 1468–1471 (2000).

[12] E Aumaitre, S Knoche, P Cicuta, and D Vella, "Wrinkling in the deflation of elastic bubbles," *Eur. Phys. J. E* **36**, 22 (2013).

[13] Er Qiang Li, Daniel Beilharz, and Sigurdur T. Thoroddsen, "Vortex-induced buckling of a viscous drop impacting a pool," *Phys. Rev. Fluids* **2**, 073602 (2017).

[14] T. Uemura, Y. Ueda, and M. Iguchi, "Ripples on a rising bubble through an immiscible two-liquid interface generate numerous micro droplets," *Europhys. Lett.* **92**, 34004 (2010).

[15] Marie Le Merrer, David Quéré, and Christophe Clanet, "Buckling of Viscous Filaments of a Fluid under Compression Stresses," *Phys. Rev. Lett.* **109**, 064502 (2012).

[16] S. M. Salili, T. Ostapenko, O. Kress, C. Bailey, W. Weissflog, K. Harth, A. Eremin, R. Stannarius, and A. Jákli, "Rupture and recoil of bent-core liquid crystal filaments," *Soft Matter* **12**, 4725 (2016).

[17] R. Stannarius, C. Cramer, and H. Schüring, "Self-Supporting Smectic Bubbles," *Mol. Cryst. Liq. Cryst.* **329**, 1035 (1999).

[18] T. Trittel, K. Harth, and R. Stannarius, "Smectic C to smectic A transition induced mechanically by rupture of freely suspended liquid crystal films," *Soft Matter* **13**, 3199 (2017).

[19] U. Kornek, F. Müller, K. Harth, A. Hahn, S. Ganesan, L. Tobiska, and R. Stannarius, "Oscillations of soap bubbles," *New J. Phys.* **12**, 073031 (2010).

[20] C. Santangelo and R. Kamien, "Curvature and topology in smectic-A liquid crystals," *Proc. R. Soc. A* **461**, 2911–2921 (2005).

[21] S Fujii, S Komura, Y Ishii, and C-Y D Lu, "Elasticity of smectic liquid crystals with focal conic domains," *J. Phys.: Condens. Matter* **23**, 235105 (2011).